Cu/CGO cermet based electrodes for

Symmetric and Reversible Solid Oxide Fuel Cells

G. Carollo,[a] A. Garbujo,[a] A. Bedon,[a] D. Ferri,[c] M.M. Natile,[b,a] A. Glisenti[a,b]

[a] Dept. of Chemical Sciences, University of Padova,

Via F. Marzolo, 1, 35131, Padova, Italy.

[b] CNR-ICMATE, INSTM

Via F. Marzolo, 1, 35131, Padova, Italy.

[c] Paul Scherrer Institut

Villigen PSI, 5232, Switzerland.

Abstract

Cu-based cermets suitable for electrodes in Symmetric and Reversible Solid Oxide Fuel Cells (SR-SOFCs) based on the Cerium Gadolinum Oxide (CGO) electrolyte were developed and successfully tested in the intermediate temperature range (600-800°C). The Cu/CGO cermets were prepared by means of a self-combustion based citrate procedure and the effects of synthesis conditions were studied. Characterization of the Cu/CGO nanocomposites by XPS, XRD, SEM, TPR suggested that this procedure allows obtaining highly dispersed CuO on the cerium gadolinium oxide. Conversion higher than 80% was observed above 600°C in methane total oxidation. Synthesis parameters affected both properties and catalytic performance. The behaviour under redox conditions was studied by operando high-energy XRD under oscillating H_2/O_2 feed. Reducing conditions converted CuO into Cu(0) passing through an intermediate Cu_2O phase while increasing the conductivity and the reactivity. This structural modification was completely reversible. The high stability, reversibility, catalytic activity and electrochemical performance make these electrodes promising for SR-SOFCs.

1 Introduction

Ni-Yttria-stabilized Zirconia (Ni-YSZ) cermets are the most traditionally diffused anodes for Solid Oxide Fuel Cells (SOFCs) but their use in direct methane fuel cells is complicated by their capability to catalyse the formation of carbon filaments that causes the efficiency loss of the device

[1]. A suitable anode for the direct oxidation of methane needs good electronic conductivity and electrocatalytic activity decoupled from the tendency to form carbon. Copper based ceria cermets demonstrated to be advantageous in replacing Ni-cermets for direct hydrocarbons SOFCs [2-6]. In these cermets the electrical conductivity is warranted by copper, whereas ceria is responsible for the catalytic activity in oxidation reactions. Moreover, $Ce_{0.9}Gd_{0.1}O_{1.95}$ (CGO) is an ionic conductor capable to operate at intermediate temperature (600-800°C), thus opening interesting opportunities for a wider application of these devices. In the present contribution, we developed and optimized a new procedure for the Cu-CGO cermet synthesis using the citrate route in order to obtain highly dispersed CuO nanoparticles in CGO.

In addition to the traditional SOFC geometry, a CGO-based symmetric configuration can be considered through the appropriate optimization of the electrodes. This approach could greatly simplify the production of fuel cells because the assembly of the electrodes can be carried out in a single thermal step, thus decreasing the fabrication costs. Even more important, compatibility issues can be minimized and the problems related to poisoning (sulphur and carbon deposition) simply addressed by reversing the gas flow. To reach this objective, beside electronic conductivity and electrocatalytic activity, stability/reversibility in oxidizing and reducing conditions is required for a successful application in symmetric and reversible SOFCs (SR-SOFCs). In this context, we decided to investigate the structural behaviour of the CuO/CGO nanocomposites under oscillating H_2/O_2 feed.

2 Experimental

2.1 Synthesis

The nanocomposites CuO/CGO (CGO = $Ce_{0.9}Gd_{0.1}O_{1.95}$; CuO:CGO = 2:3 by weight) were obtained by the citrate method [7] starting from CGO (Sigma-Aldrich >99%, particle size 5-10 nm) and CuO (Sigma-Aldrich 98%, <5 μm). Citric acid monohydrate (Sigma Aldrich >99%) was added to an aqueous solution of the copper cations obtained by mineralization of CuO with nitric acid with a molar ratio of 1.9:1 with respect to the total amount of cations. Before adding CGO powder to the solution, the pH was adjusted to 1, 4 or 8, thus obtaining three different solutions from which a different complexation and final particle dispersion is expected (the final samples will be hereafter indicated as pH1, pH4, and pH8). Each solution was than heated to 80°C in air to promote water evaporation and to obtain a wet gel. The gels were heated in air to 400°C (5°C/min heating rate) for 2 h to decompose the organic framework. At the end of the heat treatment, the powders were grinded and then calcined at 600°C for 5 h. This procedure was preferred to the traditional wet

impregnation to allow the deposition of copper oxide in highly dispersed form as a result of the complexation by citric acid.

2.2 Characterization

X-ray photoelectron spectroscopy (XPS) measurements were carried out with a Perkin Elmer Φ 5600ci Multi Technique System. The spectrometer was calibrated by assuming the binding energy (BE) of the Au $4f_{7/2}$ line to be 84.0 eV with respect to the Fermi level. Both extended spectra (survey - 187.85 eV pass energy, 0.5 eV/step, 0.05 s/step) and detailed spectra (Ce 3d, Gd 4d, Cu 2p, O 1s and C 1s – 23.5 eV pass energy, 0.1 eV/step, 0.1 s/step) were collected with a standard Al Kα source. The atomic percentage was evaluated using the PHI sensitivity factors [8] after a Shirley-type background subtraction [9]. The peak positions were corrected for the charging effects by considering the C 1s peak at 285.0 eV and evaluating the BE differences [10]. X-ray diffraction (XRD) analyses were performed with a Bruker D8 Advance diffractometer with Bragg-Brentano geometry using a Cu Kα radiation (40 kV, 40 mA, λ = 0.154 nm). Temperature Programmed Reduction (TPR) measurements were performed with an Autochem II 2920 Micromeritics equipped with a thermal conductivity detector (TCD). TPR measurements were carried out in a quartz reactor using 50 mg of the sample and heating from RT to 900°C at 10 °C/min under a constant flow of 5 vol% H_2/Ar (50 mL/min). Field emission-scanning electron microscopy and energy dispersive X-ray spectroscopy (EDX) measurements were carried out on a Zeiss SUPRA 40VP at acceleration voltages of 20 kV.

2.3 Catalytic tests

The sample (50 mg) was loaded in a glass reactor of 6 mm internal diameter and was exposed to stoichiometric CH_4/O_2 mixtures (2 vol% CH_4 and 4 vol% O_2, balance Ar) while heating from room temperature to 900°C. All gas flows were controlled by thermal mass flow meters (Vögtlin Instruments). The sample temperature was monitored by a thermocouple inserted right upstream of the bed. The composition of the gas feed was measured with an Agilent 7890A gas chromatograph equipped with a TCD and two columns (molecular sieve 13X, 60/80 mesh, 1.8 m; Porapak Q, 1.8 m). Calibration was performed using standard gases containing known concentrations of the components.

2.4 Time-resolved operando XRD

Time-resolved operando XRD measurements were performed at beamline ID 15 of the European Synchrotron Radiation Facility (ESRF, Grenoble) in the Q range of 0-12 Å^{-1} and at an energy of

74.9 keV. The patterns were collected every 0.5 s during the heating ramp and at static temperatures. Alternate pulses (20 s) of 5 vol% H_2/Ar and 5 vol% O_2/Ar were performed at 400°C in a home-made cell closed by X-ray transparent windows (graphite) [11] and interfaced with a mass spectrometer (Pfeiffer, Omnistar).

2.5 Electrochemical characterization

The electrochemical measurements were performed using symmetric cells (Cu-CGO/CGO/Cu-CGO) made of dense gadolinium doped ceria ceramics (theoretical density >96%) as electrolyte on which electrode materials based on the as prepared CuO/CGO powder were deposited as porous layers [12] and reduced by treating in 5 vol% H_2 at 400°C for 1 h. The electrolyte was produced from a pressed pellet calcined at 1500°C for 5 h at 3°C/min heating ramp. The symmetric electrode was deposited by a home-made screen printing machine and calcined on the electrolyte at 1050°C for 2 h at 2°C/min heating ramp in H_2 (5%) atmosphere. After calcination the electrode thickness was about 10 μm, as show in Figure 1.
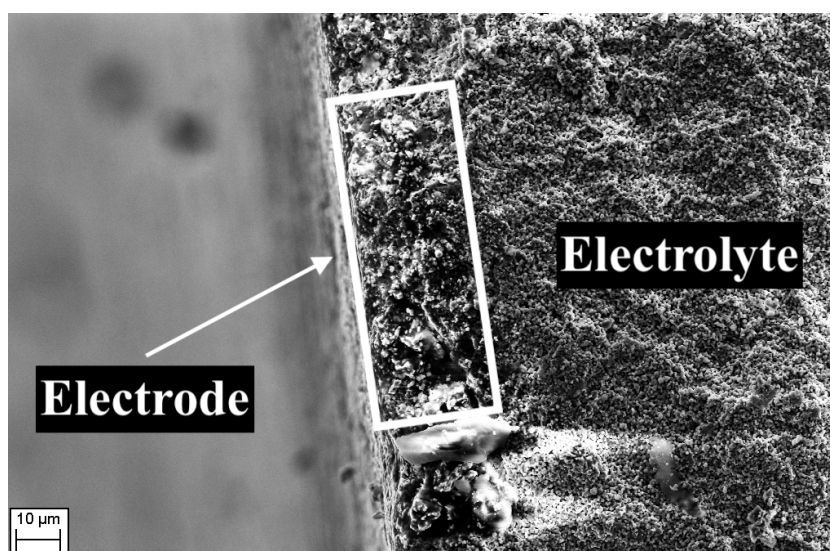

Figure 1. SEM image of cell's section.

Electrochemical Impedance Spectroscopy (EIS) measurements were carried out using an Autolab Frequency Response Analyser. The frequency scanned was from 0.05 Hz to 1 MHz and the set to amplitude 0.05 V.

3 Results and discussion

3.1 XRD

Figure 2 shows the results of the XRD analysis. The commercial CGO has an excellent crystallinity and does not show impurity within the detection limit of this analysis technique. The Cu/CGO

composite samples are characterized by the same reflections of pristine CGO, plus some other reflections that can all be related to the formation of monoclinic CuO. The pH of the precursors solution does not seem to influence significantly the final crystalline structure.
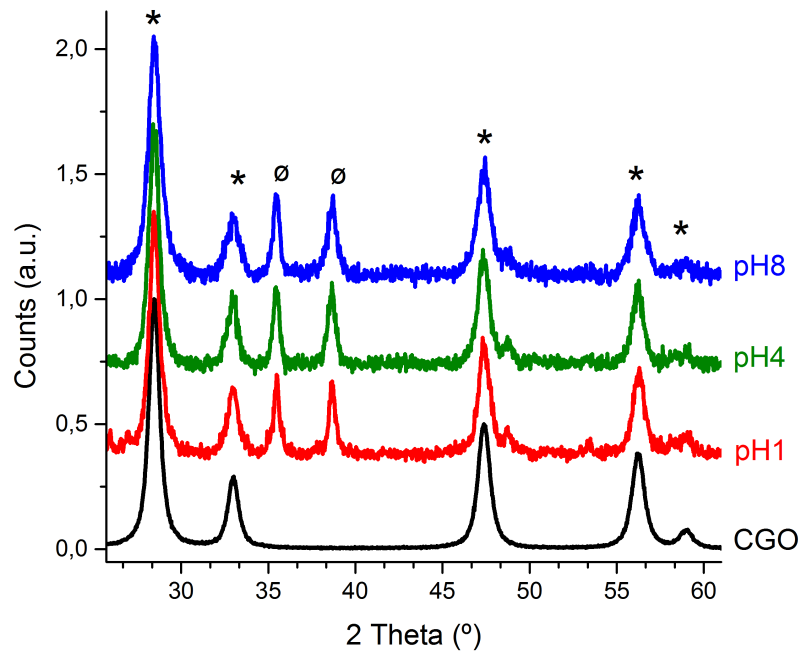

Figure 2. XRD patterns of the CuO/CGO nanocomposites obtained at increasing pH. Symbols: [*] CGO, [ø] CuO. The pattern of CGO is reported for comparison.

3.2 XPS

The Cu $2p_{3/2}$ peak position (934.1 eV) is consistent with that expected for Cu(II) [13]. Consistently, the shake up signal (about 942 eV) characteristic of Cu(II) was evident. No significant differences were observed in the Ce 3d signals after copper deposition. Concerning the XPS atomic surface compositions, in the sample prepared at pH =1 the lower amount of copper and a higher amount of Ce respect to nominal values suggest a surface substitution phenomenon.

Table 1. XPS atomic compositions (%) before and after the deposition of copper under different synthesis conditions. In brackets value without oxygen.

Sample		Ce	Gd	Cu	O	Gd/Ce	Cu/Ce
CGO	XPS	31.5 (92.1)	2.7 (7.9)	-	65.8	0.1	-
	Nominal	30.5 (90.0)	3.4 (10.0)	-	66.1	0.1	-
CuO$_x$/CGO pH 1	XPS	22.9 (55.1)	2.4 (5.7)	16.3 (39.2)	58.4	0.1	0.7
CuO$_x$/CGO pH 8	XPS	16.3 (35.0)	8.8 (18.9)	21.5 (46.1)	53.4	0.5	1.3
CuO$_x$/CGO	Nominal	15.4 (36.7)	1.7 (4.1)	24.8 (59.2)	58.1	0.1	1.6

5

3.4 SEM

Synthesis parameters, including pH, often have a deep effect on final results in this kind of syntheses. In particular, citric acid acts as a complexant only if its carboxylic groups are not hydrogenated, so with very low pH values the interaction between this molecule and metallic cations would be impossible. This behaviour is confirmed by SEM images. At pH= 1, the CuO agglomerate was inhomogeneously dispersed on the surface. The obtained CuO particle size was larger than 1 μm (Figure 3a). However, at pH= 8, the complexation of copper by citric acid induced grater dispersion with smaller particles size, i.e. < 1 μm (Figure 3b).

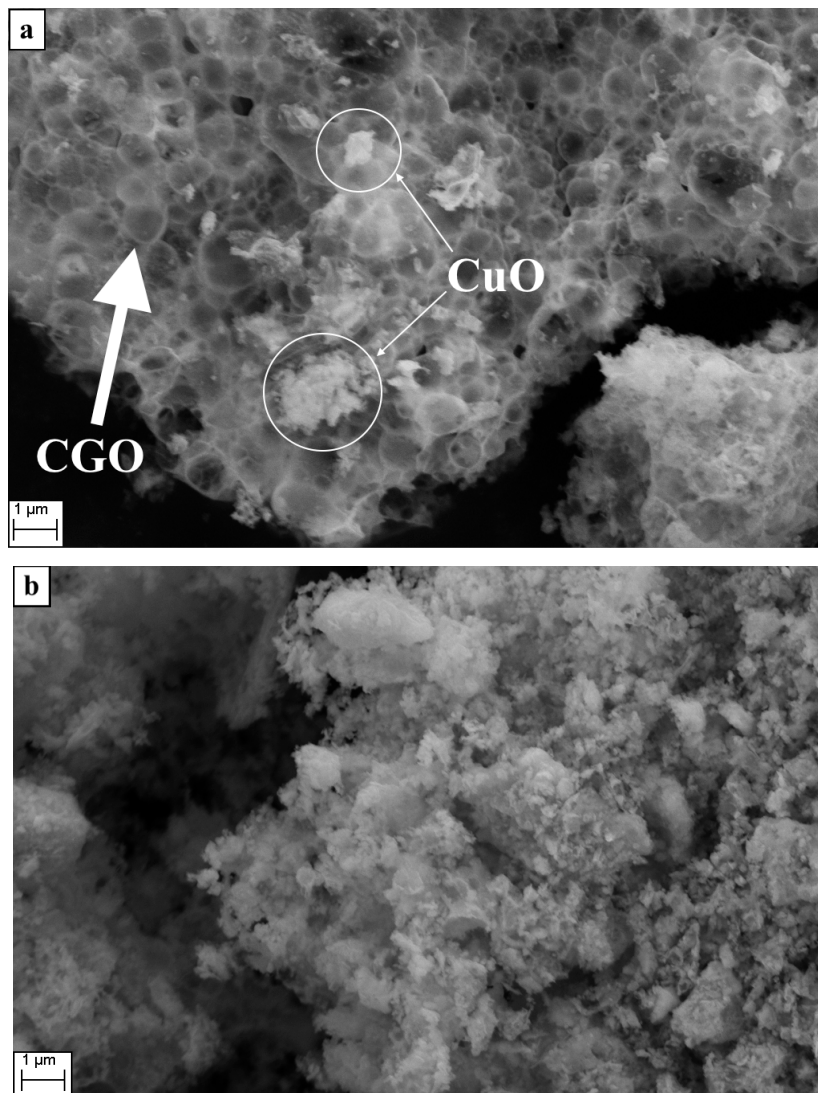
Figure 3. a) SEM image of the CuO/CGO pH1 powder; b) SEM image of the CuO/CGO pH8 powder.

3.3 TPR

On the basis of literature, pure CeO_2 exhibits two reduction peaks at 450 and 900°C (the latter being out of the sampled interval). The addition of gadolinium stabilizes cerium towards reduction, so that no signal is measured below 500°C as ceria reduction initiates above that temperature [14]. This is

confirmed also by our measurements, reported in Figure 4: no important reduction events were observed for CGO below 900°C testifying its remarkable stability under reducing conditions. The deposition of copper to form the CuO/CGO composite induces the appearance of several signals during the TPR measurements (Figure 4), which must be related directly to the presence of copper. The temperature of reduction is compatible with the Cu(II) → Cu(0) process: the corresponding signal in the CuO reference was observed at 316°C. The lower reduction temperature was consistent with the extent of dispersion of CuO [15]. The formation of mixed CuCe phases can be excluded, because in mixed CuCe oxide catalysts the reduction of copper is observed at lower temperatures and is always concluded below 275°C [16]. The data indicate that the reduction of copper oxide from Cu(II) to Cu(0) occurs in a single step without formation of a Cu(I) intermediate. This is likely true for a large fraction of copper oxide particles, but some particles probably follow a different two-steps route. This is suggested by the shoulder at low temperature (180-200°C) that is representative of the Cu(II) → Cu(I) process. Such interpretation is preferred to the formation of small mixed CuCe phases (that are reduced in the same interval) because of the results of time-resolved XRD, shown in the following paragraphs, clearly indicating the formation of Cu_2O at the same temperature. The fraction of particles reducing to Cu(I) becomes more evident with increasing the pH of synthesis. The increment of this parameter has been linked previously to the formation of increasingly dispersed particles of smaller sizes using SEM. Therefore the choice between the two possible reduction routes (two steps with Cu(I) intermediate or one step directly to Cu(0)) is probably determined by the size of the particles, with smaller ones being more prone to reduction at intermediate Cu_2O than larger ones.
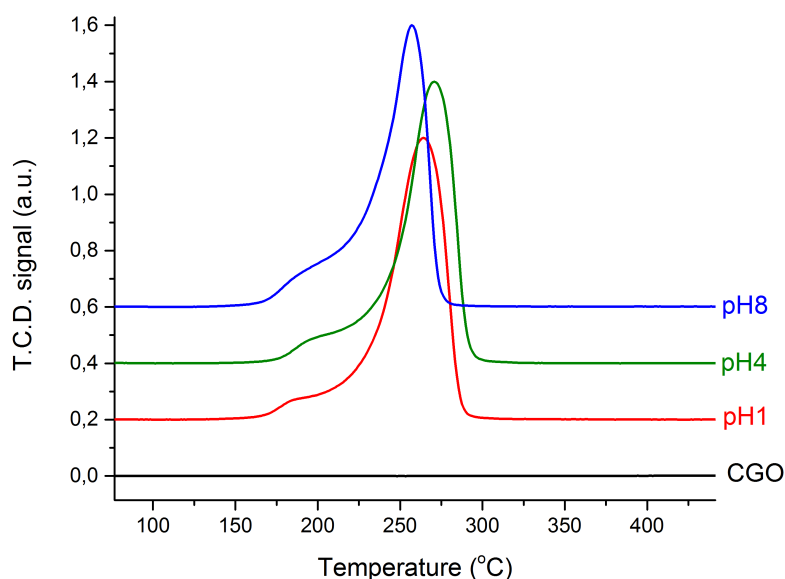

Figure 4. TPR curves of the CuO/CGO nanocomposites obtained at increasing pH. The line of CGO is reported for comparison.

7

This important result confirmed the possibility to obtain highly dispersed particles by opportunely modifying the citrate synthesis procedure.

The comparison between the estimated (123 cm^3/g) and measured (123 cm^3/g for all the three samples) H$_2$ consumption confirmed that copper was present as Cu(II).

3.6 Catalytic and electrocatalytic tests

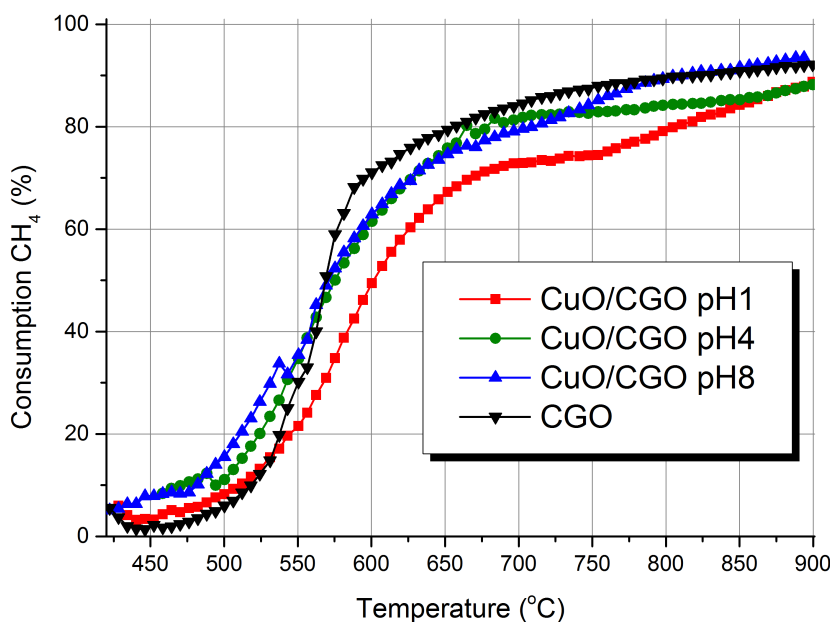The catalytic behaviour observed before and after the deposition of copper oxide is reported in Figure 5.

Figure 5. Catalytic activity in methane oxidation observed for the CGO before and after copper oxide deposition.

The onset temperature of the CGO support for methane oxidation was around 475°C; the temperature of 50% methane conversion (T$_{50}$) was 575°C and a conversion of more than 80% was reached at 650°C. Considering that the typical temperature range for SOFCs application is between 600°C and 800°C, it can be argued that this catalytic activity could be exploited in relationship with these devices. Taking in account this result, CGO can be addressed as a good catalyst for this reaction, it has a fair activity and is also fully selective towards the complete oxidation. The deposition of CuO did not decrease significantly the catalytic activity, in spite of the coverage of the CGO surface. CuO deposition was detrimental to some extent (T$_{50}$ = 600°C; 80% conversion at 800°C) only in the nanocomposite obtained at pH= 1, probably because of its very low dispersion.
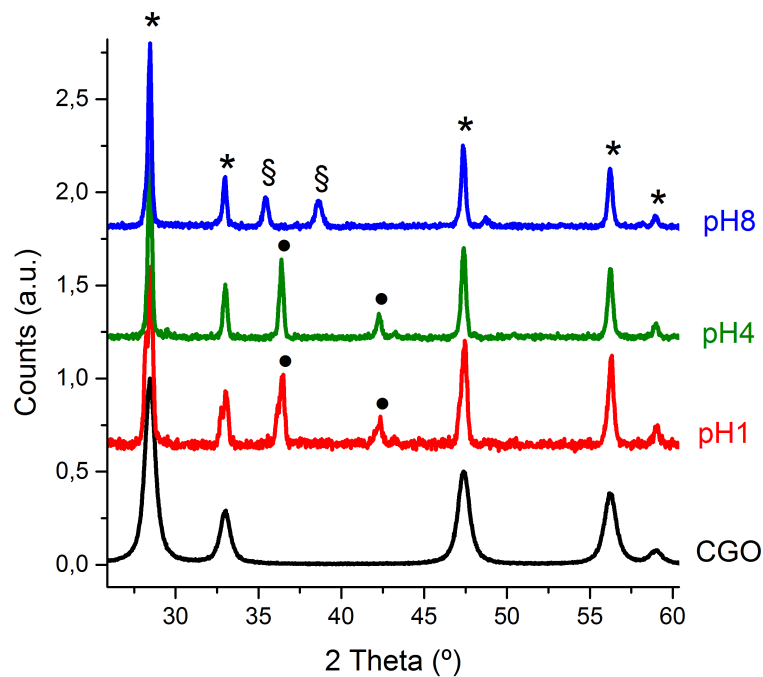
Figure 6. XRD patterns of the CuO/CGO nanocomposites obtained at increasing pH after reaction. Symbols: [*] CGO, [§] CuO, [•]Cu. The pattern of CGO is reported for comparison.

The XRD patterns obtained for the samples after the reaction are compared in Figure 6. In all cases the XRD signals were characterized by a smaller FWHM suggesting the increase of the crystallite size, but also by a better signal/noise ratio, which is related to a higher crystallinity of the samples. A different behaviour was observed between the composite obtained at pH = 8 and those prepared at pH = 1 and 4. In the former, the increase of the crystallite size was the only observed difference, whereas in the latter two nanocomposites copper was converted into the metal form. These results suggest that the synthesis at pH = 8 allows to reach a better dispersion of the CuO nanoparticles, thus a stabilizing effect originating from an intimate and extensive contact between the CGO surface and the CuO nanoparticles.

The high dispersion of copper greatly improves the electrochemical performance as a consequence of the enhanced electrical conductivity. EIS measurements confirm that the Area Specific Resistance (ASR) decreased significantly due to copper dispersion and as a function of temperature. The Nyquist plot analysis allowed to distinguish between the different contributions to the resistance and thus to optimize the electrode preparation.
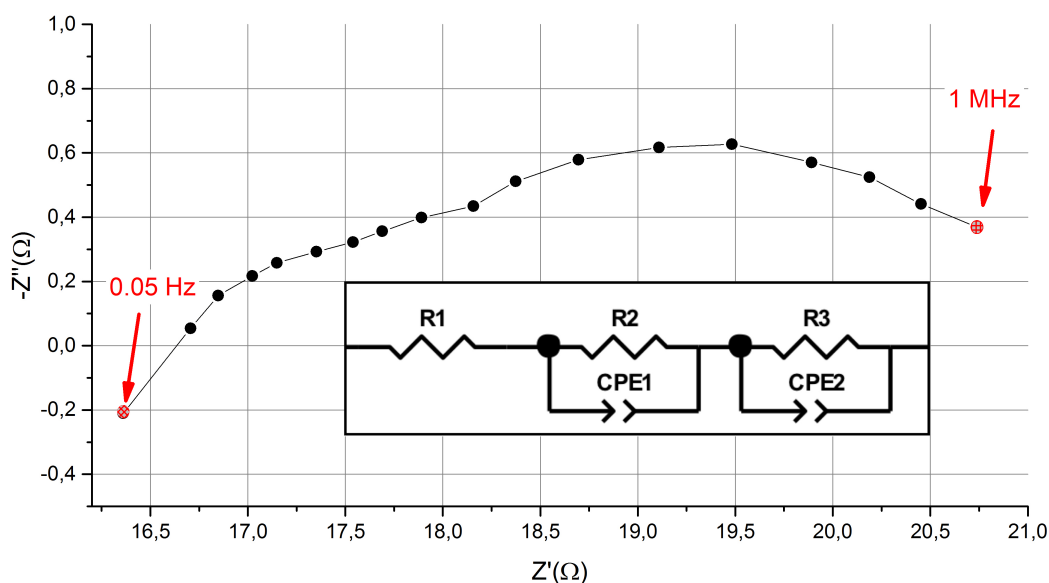
Figure 7. Impedance spectra of cermet with 40 wt.% Cu synthesised at pH = 8, temperature 800ºC under hydrogen.

A typical Nyquist plot of impedance response spectra of Cu-CGO cermet, acquired at 800 ºC under hydrogen, is shown in Fig. 7. The equivalent circuit R1(R2CPE1)(R3CPE2) was used to fit the data. In this circuit, R1 is the electrolyte ohmic resistance in series with two distinct electrode contributions consisting of resistances (R2 and R3) in parallel with constant phase elements (CPE1 and CPE2). The high and low frequency contributions can be associated with charge transfer and diffusional processes, respectively [17]. The anode area specific resistance (ASR), characterizing the electrochemical performance, was obtained from the sum of the overall electrode resistance (R2 + R3) multiplied by the electrode surface area and divided by 2, to take into account the symmetrical cell configuration. The best ASR achieved in hydrogen was 6.50 Ωcm^2 at 800ºC, a slightly high value which could be greatly improved by optimizing the device preparation.

3.6 Time-resolved XRD

The behaviour under reducing conditions was investigated in more detail by collecting time-resolved XRD patterns. The continuous perturbation of the sample by alternated gas pulses requires high time resolution to obtain kinetic information concerning the structural changes. The data collected in temperature ramp for the sample prepared at pH = 8 (Figure 8) showed the reduction of CuO to Cu through the formation of the intermediate Cu_2O phase at about 190°C, as postulated from TPR analysis (Figure 4). The Cu_2O contribution at 2.55 Å^{-1} (2θ = 36.4) appeared clearly at ca. 175°C while the CuO phase gradually disappeared. Cu_2O was only formed transiently between 180ºC and 200ºC. When the Cu phase appeared, the CuO and Cu_2O phases vanished simultaneously. The coexistence of the CuO and Cu_2O reflections at the same temperatures

confirmed that only a part of the particles followed this path, while the rest was seemingly reduced to metallic copper in a single step.
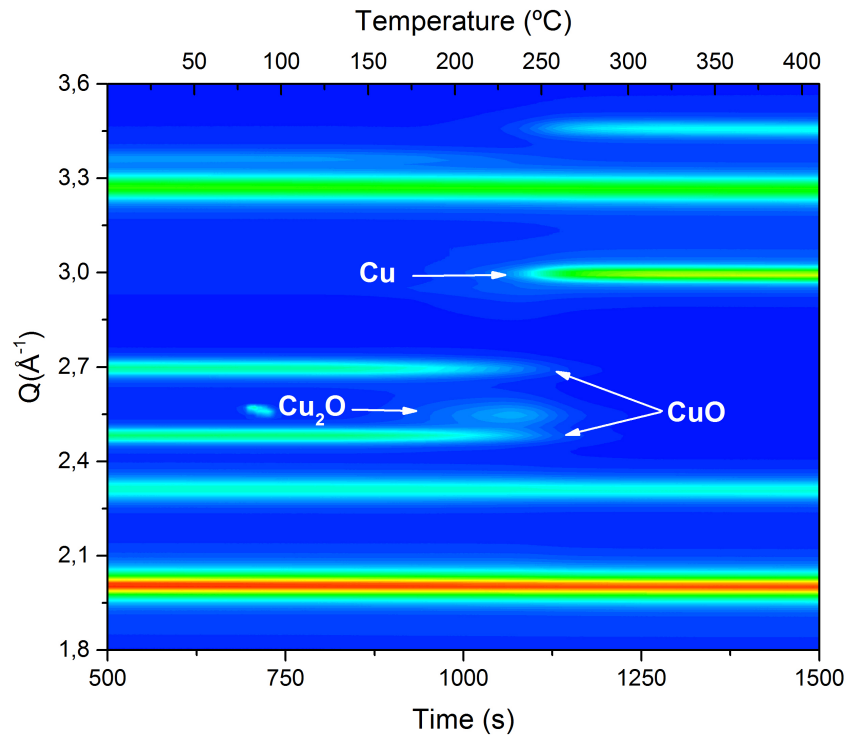

Figure 8. 2D visualization of the operando XRD data acquired during the heating ramp (50-400ºC) under 5 vol% H_2/Ar flow. Time-resolution: 0.5 s.
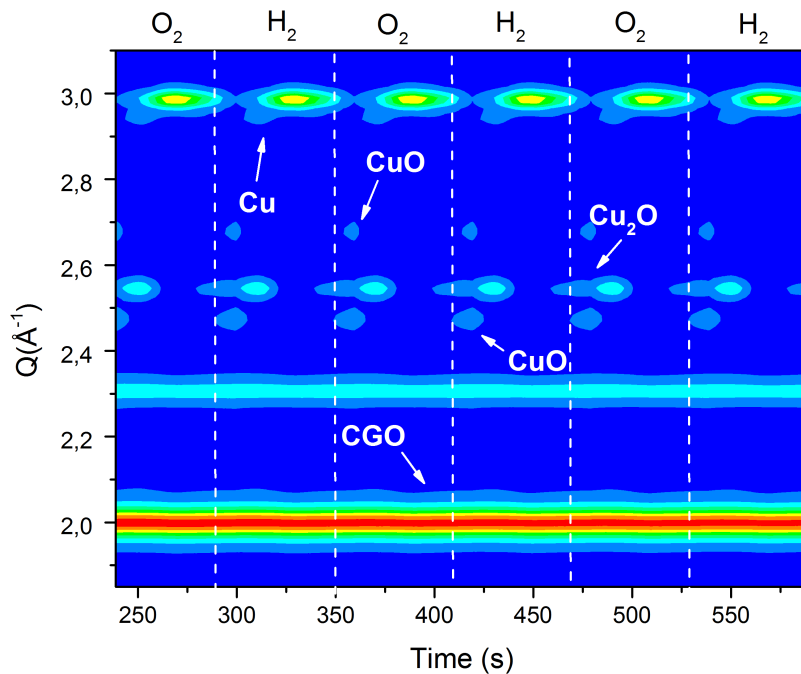

Figure 9. 2D visualization of the operando XRD data acquired during repeated and consecutive pulses of 5 vol% H_2/Ar and 5 vol% O_2/Ar at 400ºC.

As expected, the mass analysis revealed the formation of water as product when the sample was in reducing environment. During the redox pulsing (Figure 9), the copper dispersed on the CGO surface changed repeatedly and reversibly from CuO to Cu through Cu_2O in the H_2 pulse and re-oxidized reversibly in the O_2 pulse. The main XRD reflection of the CGO phase also experienced a reversible change of d spacing between the reducing and the oxidizing pulses suggesting a reversible expansion/contraction of the CGO lattice upon oxygen exchange with the environment but without loss of the structure.

4 Conclusions

In this contribution, we have developed a new procedure for the dispersion of copper oxide on CGO, and we have demonstrated that the copper distribution can be controlled through the appropriate selection of the synthesis conditions. The highly dispersed copper enhances the electron conductivity without decreasing the catalytic performance of CGO. The measurements conducted by Electrochemical Impedance Spectroscopy (EIS), showed only modest conductivity at 800ºC in hydrogen: these measurements can be deeply improved by optimizing the electrode/electrolyte interface. The X-ray photoelectron spectroscopy (XPS) measurements have showed how the synthesis parameters can heavily influence the surface of the cermet, so that the catalytic activity can be affected. Indeed, the most promising cermet was synthesized at pH = 8, where the citric acid had the best complexation capability. The structural behaviour observed by operando time-resolved XRD has confirmed the stability and reversibility of the cermet under reducing and oxidizing condition and therefore the possibility to use this material as electrode in intermediate temperature Solid Oxide Fuel Cells.

Acknowledgements

References

[1] S. Mc Intosh, R. J. Gorte; Chem. Rev. 104 (2004) 4845.

[2] S. Park, R. J. Gorte, J.M. Vohs; Applications of heterogeneous catalysis in the direct oxidation of hydrocarbons in a solid-oxide fuel cell; Appl. Catal. A. Gen. 200 (2000) 55-61.

[3] A. Hornés, D. Gamarra, G. Munuera, J.C. Conesa, A. Martinez-Arias; Catalytic properties of monometallic copper and bimetallic copper-nickel systems combined with ceria and Ce-X (X= Gd, Tb) mixed oxides applicable as SOFC anodes for direct oxidation of methane; J. Power Sources 169 (2007) 9-16.

[4] N.E. Kiratzis, P. Connor, J.T.S. Irvine; Preparation and characterization of copper based cermet anodes for use in solid oxide fuel cells at intermediate temperatures; J. Electroceram. 24 (2010) 270-287.

[5] J.J. Lee, E. W. Park, S.-H. Hyun; Performance and evaluation of Cu-based nanocomposite anodes for direct utilization of hydrocarbon fuels in SOFCs; Fuel Cells 10 (2010) 145-155.

[6] J. Marrero-Jerez, E. Chinarro, B. Moreno, J. Peña-Martínez, P. Núñez; CGO20-CuO composites synthesized by the combustion method and characterized by H2-TPR Ceram. Int. 41 (2015) 10904-10909.

[7] C. Marcilly, P. Courty, B. Delmon, Preparation of Highly Dispersed Mixed Oxides and Oxide Solid Solutions by Pyrolysis of Amorphous Organic Precursors J. Am. Ceram. Soc. 53 (1970) 56-57.

[8] J.F. Moulder, W.F. Stickle, P.E. Sobol, K.D. Bomben, Handbook of X-ray Photoelectron Spectroscopy; J. Chastain, Ed., Physical Electronics, Eden Prairie, MN, 1992.

[9] D.A. Shirley, High-Resolution X-Ray Photoemission Spectrum of the Valence Bands of Gold Phys. Rev. B 5 (1972) 4709-4714.

[10] D. Briggs, J.C. Riviere, in: D. Briggs, M.P. Seah (Eds.), Practical Surface Analysis, Wiley, New York, 1983.

[11] G.L. Chiarello, M. Nachtegaal, V. Marchionni, L. Quaroni, D. Ferri, Rev. Sci. Instrum. 85 (2014) 074102.

[12] M.M. Natile, G. Eger, P. Batocchi, F. Mauvy, A. Glisenti; Strontium and copper doped LaCoO3: New cathode materials for solid oxide fuel cells? International Journal of Hydrogen Energy 42 (2017) 1724-1735.

[13] NIST XPS Database 20, Version 3.4 (Web Version).

[14] I. V. Yentekakis, G. Goula, P. Panagiotopoulou, S. Kampouri, M. J. Taylor, G. Kyriakou, R. M. Lambert: Stabilization of catalyst particles against sintering on oxide supports with high oxygen ion lability exemplified by Ir-catalyzed decomposition of N_2O. App. Catal. B Environ. 192 (2016) 357-364.

[15] G. Perin, J. Fabro, M. Guiotto, Q. Xin, M.M. Natile, P. Cool, P. Canu, A. Glisenti; Cu@LaNiO3 based nanocomposites in TWC applications. App. Catal. B Environ. 209 (2017) 214.

[16] G. Zhou, H. Lan, T. Gao, H. Xie; Influence of Ce/Cu ratio on the performance of ordered mesoporous CeCu composite oxide catalysts; Chem. Eng. J. 246 (2014) 53-63.

[17] S.P.S. Shaikh, M.R. Somalu, A. Muchtar,; Nanostructured Cu-CGO anodes fabricated using a microwave-assisted glycine–nitrate process; J. Phys. Chem. Solids 98 (2016) 91–99.